Fast differential scanning calorimetry: new solutions in data treatment and applications to molecular glass-formers

Daniele Sonaglioni*[1,2], Elpidio Tombari[3], and Simone Capaccioli†[1,2,3]

[1] Dipartimento di Fisica "E. Fermi", Università di Pisa, Largo Pontecorvo 3, 56127, Pisa, Italy
[2] CISUP, Centro per l'Integrazione della Strumentazione dell'Università di Pisa, Lungarno Pacinotti 43, 56126, Pisa, Italy
[3]Consiglio Nazionale delle Ricerche, Istituto per i Processi Chimico-Fisici (CNR-IPCF), Via Moruzzi 1, 56124 Pisa, Italy

Abstract

Fast scanning calorimetry is an experimental technique very appreciated for its capability of suppressing reorganization processes, thanks to its wide interval of scanning rates, several orders higher than that of conventional calorimeters; nevertheless, drawbacks still exist. In this paper we propose a novel way to estimate the dynamical thermal lag by using the temperatures of maximum slope of the heat flow through the glass transition when we are not in the optimal conditions to apply the existing methods based on a reference material added on both cells of the chip or on the fictive temperature. Moreover, a novel interpretation of the heat flow losses due to the sample depending on the scanning rate sign is provided, in order to rescale the measured specific heat to that from conventional calorimetry. Finally, the use of the glass to liquid transition measured on heating is shown as a new manner to reveal static thermal gradients.

Keywords:
fast scanning calorimetry
DSC
heat capacity
thermal lag
organic glasses
glass transition

*daniele.sonaglioni@phd.unipi.it
†simone.capaccioli@unipi.it

1 Introduction

Differential scanning calorimetry is an experimental technique, well established in literatute for its reliability in the study of the dynamics and thermodynamics of a generic sample: by measuring the specific heat at a given heating rate, it is possible to study the physical state of the specimen under exam.

A great step forward was made with the invention of fast calorimeters, namely calorimeters able to measure at higher scanning rate than the previous ones. In fact, if conventional calorimeters are able to measure with scanning rate from 0.1 K/min to 500 K/min, fast calorimeters have access to rates up to 240000 K/min, with a resulting widening of the window of scanning rates of several decades. These high scanning rates allow us to better suppress crystallization or, more generally, reorganization and diffusional processes inside the sample, giving the possibility to study samples otherwise not analyzable with conventional calorimeters. Moreover, it is possible to work with samples that degrade or start reacting as a consequence of thermal stresses because, thanks to the high scanning rates, the time in which the specimen crosses the critical temperature zone is considerably reduced. Another advantage of fast calorimeters relies in the small quantity of sample needed: by using hundreds of nanograms it is possible to perform a complete study.

Apart from the advantages, there are some drawbacks related to the thermal lag and heat flow losses, that have been studied in literature since the development of this technique [1], and the socalled *smearing effects* that are known since the very beginning of calorimetry [2], and extensively studied only in recent times [3].

In this paper we decided to systematically investigate these aspects by studying three prototypical glass-forming materials, i.e. orto-terphenyl (OTP), glycerol and poly(propylene glycol) (PPG). Moreover, we propose a novel way to analyze the data collected by means of the fast calorimeter: the advantage of the latter is that it can be used to every organic system, provided that it has a glass transition process in the temperature range studied.

2 Methods

2.1 Experimental details

We used a Mettler Toledo Flash DSC 2^+, equipped with an intracooler Huber TC100, to study the specific heat of ortho-terphenyl (OTP), supplied by Fluka Chemika (99% of purity), glycerol and poly(propylene glycol) ($M_w = 4000\ Da$) (PPG4000), both provided by Sigma-Aldrich (both with purity of 99.5%).

We employed the $UFS-1$ measuring chip, with an active area of 0.5 mm of diameter. The samples were placed at the center of the measuring area of the chip furnace with a thin hair. The sensor has been conditioned according to manufacturer's indications before use (see Sec.1.2.3.3 of [1]). The absolute scale of temperature has been calibrated with reference standards, i.e. adamantane, water, stearic acid and indium, all provided by Sigma-Aldrich. Measurements have been carried out under a nitrogen flux of around 5 ml/min with the support temperature set to 173 K, otherwise explicitly stated.
Conventional calorimetric measurements have been made with a Perkin Elmer model 8500, equipped with Intracooler III as refrigerating system.

2.2 Thermal lag evaluation

In general, thermal lag is a consequence of heat propagation inside the calorimetric cell and throughtout the sample and these processes need a characteristic time. In fact, there exists a typical time for heat propagation inside the sample that depends on the material under exam and on its geometry[4]. It is common knowledge that the thermal lag, T_{lag}, of the FDSC, which is the temperature difference between the sample, T, and the sensor temperature, T_{exp}, is determined almost exclusively by the sample and its contact to the sensor and is proportional to the scanning rate q, according to:

$$T_{lag} = T_{exp} - T = q \cdot \tau_{lag}, \tag{1}$$

where τ_{lag} is the characteristic time of heat transfer between the sample and the sensor [1]. Usually, thermal lag is considered a linear function of the scan rate, but second-order effects in its rate dependence have been demonstrated experimentally when spanning several decades [5] or when using high masses [6]. **Another source of non linearity of T_{lag} is the change in the specific heat of the sample within the temperature ramp, which results in an extra contribution to τ_{lag} and, as a consequence, a deformation of the shape of the measured curve [7].**
In FDSC, for each material and for each deposition of the same material on the sensor, we end with a different value of the thermal lag, due to the dependence on the sample geometry which determines the contact with the sensor and the volume within which the heat propagates. Consequently, it would be necessary to add a temperature reference material (e.g. indium) to the sample [8] or to use a significative "temperature" related to the specific process under exam, as for example the fictive temperature for the glass transition [9].
To explore the dynamical behavior of a glass, it is necessary to vary the scanning rate q. As a consequence, the experimental data will contain a different thermal lag, according to eq.1, which has to be determined *a priori* in order to extract the true sample response to different scanning rates, which

appears as a shift of the transition to higher temperature and an increase in the broadening of the heating and cooling curves to higher scanning rates, due to the temperature dependence of the internal dynamics.

To illustrate the main characteristics of the thermogram changes as a function of the scanning rate, we adopted two theoretical models, frequently used to describe the behavior of a glass. As a simplest case, we have chosen the Tool-Narayanaswamy-Moynhian (TNM) model as formulated by Hodge [10], based on an Arrenhius dependence of the characteristic relaxation time, and the extended TNM (E-TNM), where the temperature behavior of the characteristic relaxation time is reproduced by the Vogel-Fulcher-Tamman law, proposed by Weyer et al. [11] (see Supplementary Materials for further information on the models). The latter, is more suited when studying a system in a wide scan rate span, where the non-Arrhenius behavior of the characteristic relaxation time [12] has to be taken into account. **We point out that the use of the TNM model, which is one of the existing models qualitatively describing the shapes of the glass transition thermograms in relation to the activation energy, the non-linearity parameter, the relaxation time distribution, is here used to provide an example of the main changes (temperature shift and broadening) of the thermograms when the scanning rate is changed. We want to stress that the TNM and E-TNM models have been used only for descriptive purposes, and, in principle, every theoretical model describing the glass transition, could have been used because the thermal lag method we are going to introduce makes use of particular points of the experimental thermogram, which are model independent. The test of this method has been based on the comparison of the obtained results with those calculated with the well-established fictive temperature method, as we will show in Sec.3.1.**

In both models, the sample is ideal, i.e. point-like and without thermal lag. The model parameters were obtained after fitting an experimental curve at 100 K/s for OTP and checking that the obtained values were close to the ones reported in literature (see fig.$S1$ and Tab.$S1$ of the Supplementary Materials for more information).

The main panels of fig.1 report the results of the simulations on two decades of scanning rate made with the two models.

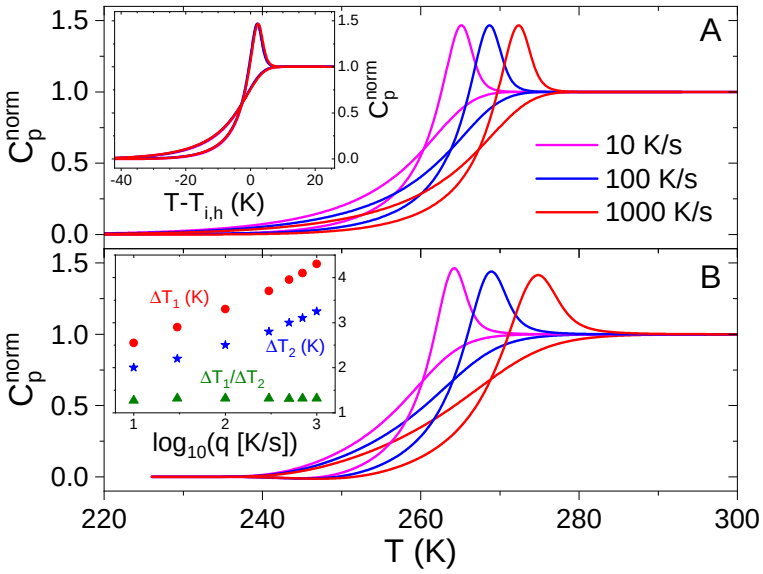

Figure 1: Panel A: Normalized specific heat from TNM simulations. Inset: Normalized specific heat curves rescaled in temperature by subtracting in x-axis the temperature of the maximum specific heat rise on heating.
Panel B: Normalized specific heat from E-TNM simulations. Inset: Temperature difference between heating and cooling specific heat slope (ΔT_1) and temperature differences between the temperature at which the overshoot appears on heating and the temperature of maximum slope on heating (ΔT_2).

The simulations with the TNM model show that, in absence of thermal gradient across the sample, the shape of the glass transition, including the overshoot peak, remains the same independently on the scanning rate, and the curves shift to higher temperature at higher scanning rates, as it is possible to notice in fig.1A. For the E-TNM model, the shape of the cooling and heating thermograms shows a broadening and a temperature shift for high scanning rates, simultaneously to a decrease of the amplitude of the overshoot peak of the heating curve, as it is possible to notice in fig.1B. The broadening of the thermograms on increasing the scanning rate has been confirmed by several experiments on different samples [12, 13]. The origin of the broadening can be attributed to the activation enthalpy variation with temperature and to the change of distribution of the relaxation times, together with the occurrence of internal thermal lag to the sample. The latter, has been experimentally studied by Toda [3] and theoretically modeled for FDSC by Svoboda [14].
Experimentally, when the scan rate is changed, a different value of the thermal lag would be obtained, according to eq.1. The correction consists in a rigid temperature shift of the experimental thermogram for a quantity equal

to the thermal lag, which is a negative shift on heating and a positive shift on cooling. Here we propose an alternative approach to the fictive temperature (T_f), a method widely used to determine the thermal lag for glass-formers [9]. The new method here proposed aims to overcome the main limitations of the T_f method, i.e. the needing of well-extended glassy and liquid lines that are not always possible to measure. It uses a combination of significative temperatures related to the glass transition process, which are T_h and T_c that correspond to the minimum and maximum of the derivative of the heat flow versus temperature on heating and cooling, respectively, and T_{ov} that is the maximum of the overshoot peak on heating. We chose these points because these temperature positions are significative of the thermograms position and of their broadening. Moreover they are the less influenced by the superposed heat flow losses in the experimental heat flow curves because they correspond to peaks in the heat flow or in its first derivative with respect to the temperature.

An example of determination from experimental raw heat flow versus temperature data is reported in fig.2.

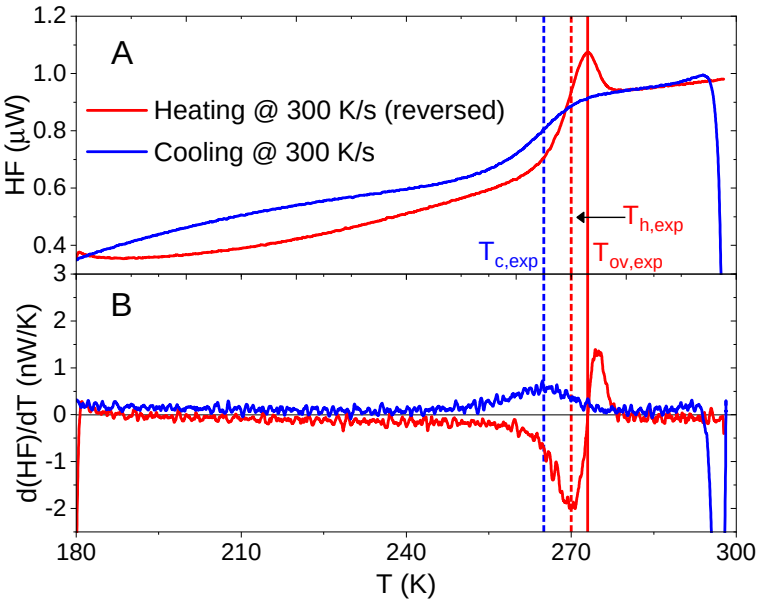

Figure 2: Panel A. Raw heating and cooling heat flow thermograms at 300 K/s for OTP. Heating scan has been vertically reversed. It is possible to notice the sigmoidal-shape of the glass-transition, both on cooling and heating, and in the temperature range $190-245$ K there is a smooth curvature due to spurious heat loss contributions. Panel B. Calculation of points of maximum slope during symmetrical heating and cooling. Vertical dashed lines indicate the points of maximum inflection on heating (red line) and cooling (blue line). Full line indicates the overshoot temperature position, which is identified as the point of maximum of heat capacity or zero crossing point of the heat flow derivative curve.

These three temperatures can be combined in two temperature differences, as follow:

$$\Delta T_1(q) = T_h(q) - T_c(q), \tag{2}$$

$$\Delta T_2(q) = T_{ov}(q) - T_h(q). \tag{3}$$

These differences, when refferred to the models, are not affected by the temperature shift of the thermogram due to the scan rate but only by the broadness of the heating and cooling curves.
As shown in the inset of fig.1A, the TNM thermograms can be fully superposed by a rigid temperature shift. As a consequence, in the case of TNM model ΔT_1 and ΔT_2 are q-independent. On the contrary, as shown for the E-TNM thermograms in the inset of fig.1B, ΔT_1 and ΔT_2 increase with the increase of the scanning rate and this means that the broadening increases. It is worth noticing that their ratio, also reported in the inset of fig.1B, is constant and invariant to the activation energy changes simulated by the E-

TNM: this means that the progressive temperature broadening of the cooling and heating curves on increasing the scanning rate does not affect the ratio $r = \Delta T_1/\Delta T_2$.

When the equivalent temperatures of T_c, T_h and T_{ov} are determined on the experimental curves at a certain q, i.e. $T_{c,exp}$, $T_{h,exp}$ and $T_{ov,exp}$, they are all affected by the same thermal lag, with positive sign for the heating curve and negative one for the cooling. On defining $\Delta T_{1,exp} = T_{h,exp}(q) - T_{c,exp}(q)$ and $\Delta T_{2,exp} = T_{ov,exp}(q) - T_{h,exp}(q)$, and combining with eq.2 and eq.3, we obtain:

$$\Delta T_{1,exp}(q) = \Delta T_1(q) + 2q \cdot \tau_{lag}, \tag{4}$$

$$\Delta T_{2,exp}(q) = \Delta T_2(q). \tag{5}$$

We notice that $\Delta T_{2,exp}(q)$, under the hypothesis of eq.1, is not affected by the thermal lag because both temperatures belong to the heating curve and allows to reveal the broadening of the curves when the scan rate is increased. When there is no significative broadening, i.e. when $\Delta T_{2,exp}(q)$ results nearly constant, τ_{lag} can be derived from eq.4, as the slope of the linear fit of $\Delta T_{1,exp}(q)$ versus q, being also $\Delta T_1(q)$ constant due to the absence of the curve broadening. We call this procedure *First Derivative Method* (FDM), because $T_{c,exp}$, $T_{h,exp}$ can be revealed as the temperature at which the first temperature derivative of the measured heat flow shows its minimum on heating and maximum on cooling (see fig.2 for a practical example). In presence of a significative broadening, revealed by $\Delta T_{2,exp}(q)$, considering that $\Delta T_1(q) = r \cdot \Delta T_2(q)$, as shown in the inset of fig.1B, and combining with eq.4 and eq.5, one obtains:

$$\frac{\Delta T_{1,exp}(q)}{\Delta T_{2,exp}(q)} = r + \frac{2q}{\Delta T_{2,exp}(q)} \cdot \tau_{lag} \tag{6}$$

Experimentally, the quantities r and τ_{lag} can be estimated through a linear fitting of the data according to eq.6. We call this protocol *Extended First Derivative Method* (E-FDM).

In Sec.3.1 we will test the compatibility of the results obtained with FDM and E-FDM, by using methods based on the energy conservation of the glass transition process. [9].

2.3 Evaluation of heat flow losses

An important issue to be overcome is the correction of unwanted couplings between the sample and the external environment: these interactions create an heat flow from the sample to its surrounding, which is generally called *heat flow loss* [1].

We have verified that the differential calorimeter, realized on the chip, is well balanced, that means that the empty reference cell and the empty furnace cell have negligible differences in heat capacity and losses to the surrounding.

This has been verified by measuring, at different scanning rates, the heat flow in the temperature interval of interest. We have found that the heat flow asymmetries between the two empty cells, i.e. reference and furnace, are two orders of magnitude smaller than what measured in presence of the sample, at the same scanning rate.

In principle, if there is no sample in the furnace cell, the measured heat flow is equal to zero but the addition of the sample on the furnace cell, from the point of view of the heat balance equations, appears with two contributions:

$$HF = mc_p q + HF_{loss}(T, q), \tag{7}$$

where the first term in the right-hand side of the equation is the heat capacity contribution, proportional to the mass m of the sample, the scanning rate q and its specific heat c_p, whereas the second term represents the heat flow losses due to the sample. **The second term is typically represented by depending only on the temperature T [15, 16, 17]: within this strict hypothesis, one should experimentally observe an heat flow loss independent from the scanning rate, but this is not the real case, so for each rate a different loss is used. Consequently, we have explicitly introduced the scanning rate dependence of the heat flow losses. In particular, tha scanning rate can contribute in two ways: the first is to influence the non-adiabaticity of the measurements and the second is to influence the thermal gradients between the sensor, the sample and the membrane in contact with them (non-stationarity).**

Within this scheme, we approximate the $HF_{loss}(T, q)$ as a sum of two terms, taking into account the two above-mentioned effects, in the following way:

$$HF_{loss}(T, q) = HF_0(T, |q|) + \kappa(T)q, \tag{8}$$

where $HF_0(T, |q|)$ is the component, influencing the non-adiabaticity, hypothesized dependent on the scanning rate modulus, while $\kappa(T)$ is the coefficient of the scanning rate sign-dependent term, which is considered to take into account the effects of the thermal gradients. As we will show later, the $\kappa(T)q$ term will appear as an extra contribution to the measured heat capacity of the sample.

Thus, if we consider separately the heating and cooling scan, the balance equation can be written as in eq.9.

$$\begin{aligned} HF_h &= mc_p|q| + HF_0(T, |q|) + \kappa(T)|q| \\ HF_c &= -mc_p|q| + HF_0(T, |q|) - \kappa(T)|q|. \end{aligned} \tag{9}$$

It is possible to notice that, by applying the semisum of the two equations in eq.9, we obtain the component of heat flow loss independent from the scan rate sign:

$$HF_0(T, |q|) = (HF_h + HF_c)/2. \tag{10}$$

The correction of this contribution is usually done via the *symmetry line*, as previously described by Schick and coworkers [15, 16], and schematically represented in fig.3.

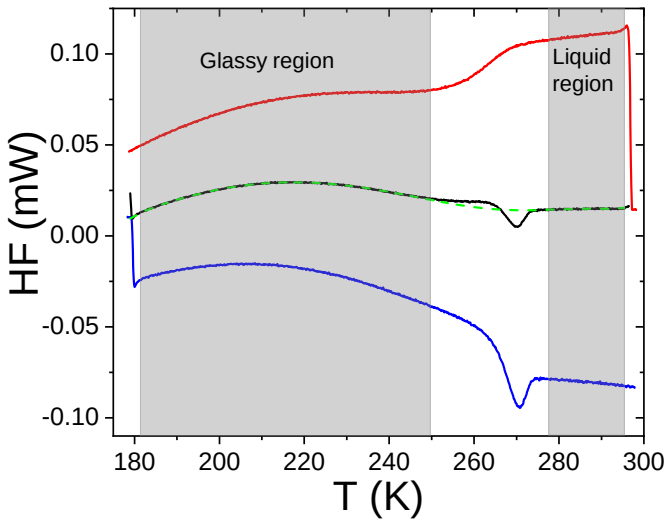

Figure 3: Example of correction procedure for OTP at 100 K/s. Red and blue lines are, respectively, cooling and heating scans, black line is the semi-sum. The green dashed line represents the resulting HF_0 obtained by fitting the two portions of the black line, delimited by the gray zones, which correspond to the region where the sample is in the glassy state (left) and liquid state (right). The degree of the polynomial used for the fit of the symmetry line is usually between 5 and 7.

The heat flow loss correction was further explored by Quick et al. with the formulation of the *slow-rate approach*: even though the method permits to obtain meaningful thermograms, deviations between the FDSC and DSC specific heat still exist. [17].
Using the symmetry line approach, by subtracting HF_0 to the heat flow measured on heating (the same applies also for the cooling), and dividing for the scanning rate, we can write:

$$C_{FDSC} = (HF_h - HF_0)/q = mc_p + \kappa(T). \tag{11}$$

It is worth noticing that C_{FDSC} is the quantity that is typically computed and that $\kappa(T)$, i.e. the scanning rate sign-dependent losses, enters in eq.11 as an extra heat capacity contribution. We model the second right-hand side term in eq.11 by a first-order polynomial approximation in T:

$$C_{FDSC} = (HF_h - HF_0)/q = mc_p + \kappa_0 + \kappa_1 T, \tag{12}$$

where κ_0 and κ_1 are the first two term of the linear expansion of $\kappa(T)$.

In the following section, we first explore the goodness of the two proposed methods to estimate the thermal lag, then we will describe the procedure to determine $\kappa(T)$, and simultaneously estimating the mass of the sample, by using the extrapolated liquid and glassy lines separately determined by the conventional DSC data.

3 Results and discussion

In this section we will expose the results obtained with the first derivative method (FDM) and the extended first derivative method (E-FDM) exposed in Sec.2.2. As a first example, we have used OTP as a benchmark, and made measurements with scanning rates between 30 and 1000 K/s. The same dataset has been used for the specific heat determination, according to eq.10 and eq.12.

3.1 Test of thermal lag correction method

In fig.4A we report the experimental and simulated values of all the above-mentioned significative temperatures, i.e. obtained from the experimental raw heat flow data measured at different scanning rate and from the simulations with the E-TNM model for OTP. In fig.4B and 4C we report the elaborations of the experimental data of fig.4A according to the FDM and E-FDM models, respectively.

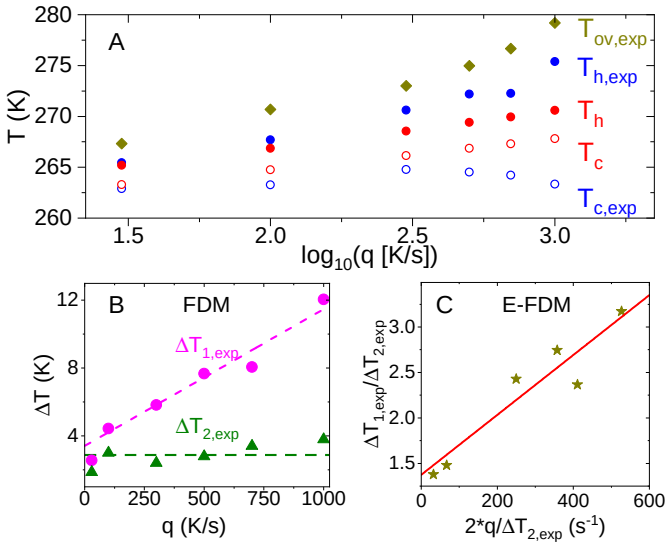

Figure 4: Panel A. Points of inflection of heat flow on heating (full points) and cooling (open points) both for experimental (blue points) and for simulations with the E-TNM model (red points) for OTP. Green diamonds are the experimental overshoot temperatures $T_{ov,exp}$. Panel B. Experimental temperature differences of the inflection temperatures on heating and cooling $\Delta T_{1,exp}(q)$ (magenta points) and between the overshoot maximum and the inflection point on heating $\Delta T_{2,exp}(q)$ (green triangles). Dashed magenta line is the linear fit of $\Delta T_{1,exp}(q)$. Green dashed line represents the average value of $\Delta T_{2,exp}(q)$. In this case the analysis is based on the framework of FDM. Panel C. Linear fitting of the $\Delta T_{1,exp}(q)$ and $\Delta T_{2,exp}(q)$ combination according to eq.6 in the framework of E-FDM.

We decided to use both models for the OTP data analysis, graphically reported in figs. $4B$ and $4C$, because $\Delta T_{2,exp}(q)$ can be tought both constant and q-dependent, as its observed variation is of the order of 1 degree with respect to its average value, so it is slight in the two decades explored in the current study. From the linear fitting of $\Delta T_{1,exp}(q)$ with the FDM model we estimated, according to eqs.4 and 5, a value of $\tau_{lag} = 4.03\ ms$. On the other side, according to the E-FDM model, i.e. using eq.6, we obtained $\tau_{lag} = 3.3\ ms$, with a discrepancy of $\simeq 0.7\ ms$.
By means of the FDM and E-FDM, followed by the subtraction of the symmetry line, we are able to correct the experimental thermograms, and thereafter we have made some cross-checks in order to verify which method gives more physically meaningful results.
As a first cross-check, we calculated the area under the heating and cooling scans taken at the same rate. In fact, the glass transition is a reversible process, thus all the energy subtracted to the sample during cooling has to

be provided on heating, so the areas under the heating and cooling thermograms must be the same, provided that the rate is the same [9]. To better compare the areas at several scan rate, we have defined an objective function, in a way that, the better the correction, the closer to zero is its value. The function formula is:

$$f = (A_{heat} - A_{cool})/[(A_{heat} + A_{cool})/2], \tag{13}$$

where A_{heat} and A_{cool} are, respectively, the areas under the heating and cooling scans.

We have made a further check by optimizing the thermal lag in order to minimize the objective function value. The results of these three checks are reported in fig.5.

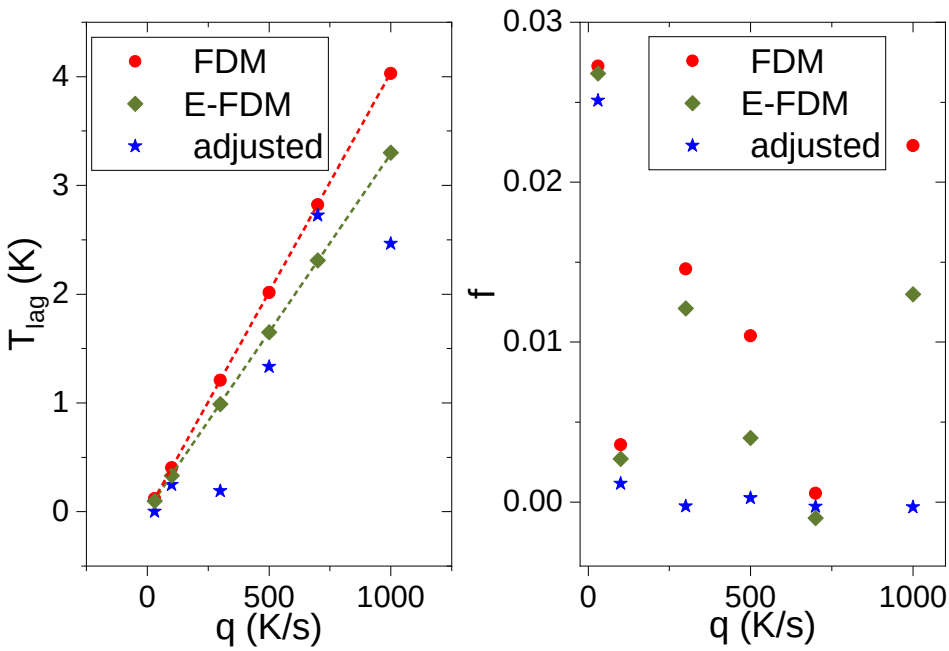

Figure 5: Left panel: Thermal lag as estimated from FDM (red points), E-FDM (green diamonds) and from optimization (blue stars) for OTP in order to set to zero the objective function. Red and green dashed lines are guides for the eye. Right panel: values of the objective function after estimation of the thermal lag from FDM (red points), E-FDM (green diamonds) and from optimizating of the thermal lag to put the objective function equal to zero (blue stars).

As it is possible to notice in the right panel of fig.5, the thermal lag estimated with the E-FDM gives an objective function closer to zero than FDM, even at low scanning rates where the correction with the symmetry line is difficult due to the low signal to noise ratio. Moreover, the thermal lags defined by optimization, shown in the left panel of fig.5, are in better agreement with the values estimated from the E-FDM. Thus, in the remaining part of the paper we will use the E-FDM to make our analyses. It is worth noticing that the maximum T_{lag} difference between FDM and E-FDM is of 0.7 K at 1000 K/s, which is very close to the experimental error, at least up to this rate.

To have a better insight within this energy-based correction procedure, we have also computed the fictive temperatures (T_f) on heating and cooling, after the temperature correction from E-FDM has been applied. T_f is defined as [18]:

$$\int_{T^*}^{T_f} (C_{p,l} - C_{p,g}) dT = \int_{T^*}^{T'} (C_p - C_{p,g}) dT, \tag{14}$$

where $C_{p,g}$ and $C_{p,l}$ are the fitting lines for, respectively, the glassy and liquid portions of the thermogram, T^* and T' are two temperatures, respectively, well above and below the transition region.

In absence of thermal lag to be corrected, as a consequence of the energy conservation, the fictive temperatures calculated upon heating and cooling must be the same [9, 19]. Thus, if the correction with the E-FDM is correct, we should obtain the same T_f on heating and cooling. The results of this test on the corrected thermograms (see fig.$S2$ Supplementary Materials for details on the T_f calulation), are reported in fig.6, together with the simulation of the fictive temperatures for OTP obtained with the E-TNM model introduced in Sec.2.2. To improve the validation of the test, we have made a measurement on another OTP sample, with a lighter mass estimated to 82 ng (see Sec.3.2 for details on mass estimation). This measurements was motivated by the fact that for the first sample of 617 ng we stopped at 298 K, so that at the highest rate the liquid line was distorted by the transient region of the cooling ramp. In this new measurement, we extended the scan to 313 K, obtaining a sufficiently wide temperature interval for the liquid line up to 1000 K/s. The τ_{lag} estimated with the E-FDM is equal to 2.2 ms, **which gives rise to a $T_{lag} = 2.2$ K at 1000 K/s. This value is in line with the one of about 1.5 K present in literature for a polystyrene sample with a mass of 90 ng [9]. The differences can be attributed to the different material under study in terms of specific heat and thermal conductivity and the difference in the temperature range of the two studies.** Note that in the whole paper we will report the results for the heavier mass.

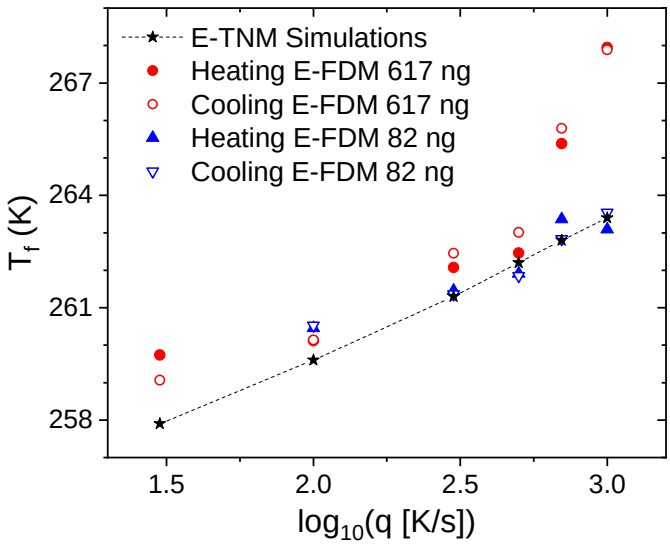

Figure 6: Simulated fictive temperature by means of E-TNM model (black stars), experimental heating (full symbols) and cooling (open symbols) fictive temperatures obtained after T_{lag} correction with the E-FDM for two samples of different mass as a function of the logarithm of the scanning rate for OTP.

The temperature shifts of the thermograms estimated with the E-FDM is confirmed to be correct because of the coincidence, within the experimental uncertaintes, of the fictive temperatures on heating and cooling. Note that, for the heavier sample, at the lowest scan rate there is a difference in the fictive temperatures of around 1 degree, which can be attributed to the low signal-to-noise ratio, that makes the thermogram correction difficult. In the lighter sample, the 30 K/s fictive temperatures data are missing because too noisy due to the smallness of the mass. Moreover, there is a discrepancy between the fictive temperatures of the two sample at 700 K/s and 1000 K/s, attributable to the fact that for the heavier sample the liquid line was distorted by an extra contribution from the transient region of the cooling ramp.

Another aspect to highlight is that the raw heat flow data (without previous thermal lag and symmetry line corrections) we measured for OTP cannot be used to estimate the fictive temperature because the heat flow losses create a non negligible distorsion (curvature) in the thermograms, more pronounced at low scan rates, as can be noted by inspecting the glassy regions in fig.2 and fig.3.

3.2 Specific heat determination

In this section we will explicitly deal with the thermograms that we have previously corrected with the E-FDM and the symmetry line subtraction. As mentioned in Sec.2, we have performed symmetrical heating and cooling from 30 to 1000 K/s in the region between 173 and 298 K, setting the temperature of the sensor support at 173 K.

Once the E-FDM and the correction for the symmetry line (see eq.10) have been applied to the heating ramps, we obtain the heat capacities reported in fig.7.

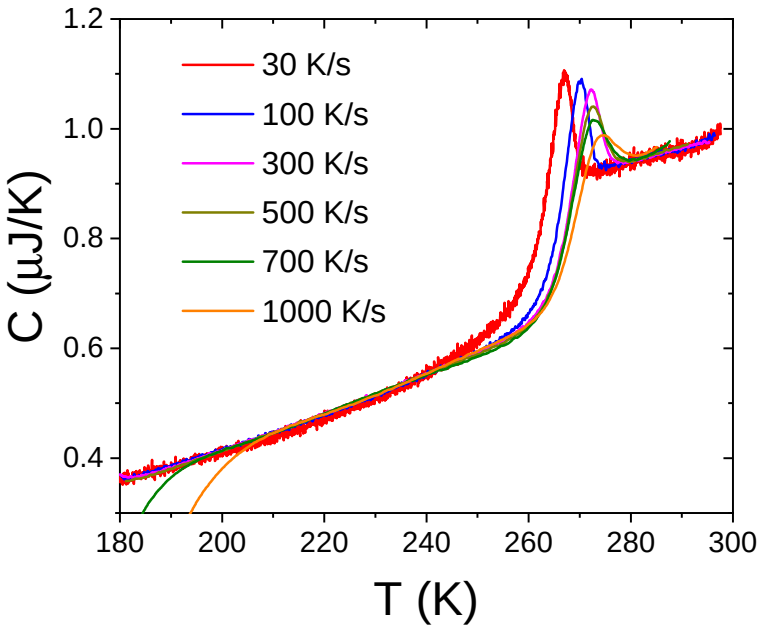

Figure 7: FDSC OTP heat capacity at different scanning rates.

As it is possible to see from fig.7, the thermograms for different scanning rates superpose very well in the glassy and liquid regimes. It has to be reminded that the heat capacity reported in fig.7, according to eq.12 corresponds to $C_{FDSC} = mc_p + \kappa_0 + \kappa_1 T$, where κ_0 and κ_1 are the coefficients of the linear equation approximating the sample losses dependent on the sign of the scanning rate. The two regions, i.e. glassy and liquid, can be measured with conventional DSC: thus the quantitative comparison between the data coming from the two techniques, i.e. FDSC and DSC, can give us the magnitude of the deviation between the two data set, quantifying the effect of the $\kappa(T)$-term contribution on the FDSC scans.
By recalling eq.12, in the liquid and glassy regions, we can write the following two equations:

$$\begin{aligned} C_{FDSC}^{liquid} &= mc_{p,DSC}^{liquid} + \kappa_0 + \kappa_1 T, \\ C_{FDSC}^{glass} &= mc_{p,DSC}^{glass} + \kappa_0 + \kappa_1 T. \end{aligned} \tag{15}$$

By applying eq.15 it is possible to estimate m, κ_0 and κ_1 by fitting the simultaneous superposition of the liquid and glassy lines of C_{FDSC} and $c_{p,DSC}$, both extrapolated in their liquid and glassy temperature intervals.
We want to stress the role of the mass parameter m which, as in [1], is estimated by comparing the glass to liquid step in FDSC heat capacity and the glass to liquid step in DSC specific heat. In the approxymation that $\kappa(T)$ is independent of the state of the sample (glassy or liquid), it is still possible to estimate the mass of the sample used for the FDSC measurement, by comparing the glass to liquid step in heat capacity at the glass transition with the one in specific heat at the glass transition measured by DSC, as prescribed in [1]. In particular, the DSC glass to liquid step to be considered is the difference between the extrapolations of the liquid and glassy lines, evaluated at the glass transition temperature of the FDSC measurement. Thus, a different glass to liquid step for each rate needs to be computed. The procedure for mass estimation is schematically represented in fig.8.

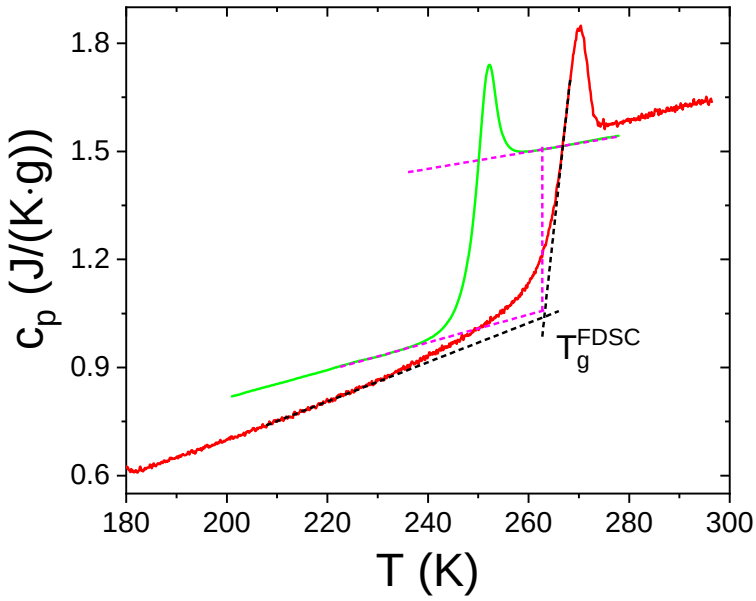

Figure 8: Estimation from the DSC thermogram (green line) of the jump in heat capacity in correspondence of the FDSC T_g for the 100 K/s ramp (red curve). Vertical purple line represents the jump in specific heat of the DSC curve in correspondence of T_g^{FDSC}. Dashed purple lines are the extrapolation of DSC liquid and glassy lines. Dashed black lines are used to estimate the T_g^{FDSC}. Note that, for the FDSC scan, the data shown correspond to $(C_{FDSC} + \kappa(T))/m$, where m is the value of the mass estimated for the 100 K/s scan by comparing the glass to liquid jump of the FDSC and DSC scans, as described in the text.

As it is possible to notice in fig.8, the FDSC liquid and glassy regimes do not agree with the DSC glassy and liquid regimes. It is possible to note that the linear extrapolations of the liquid and glassy regimes for the DSC and FDSC are not superposed and there are deviations up to 20%: in order to recover this agreement, it is sufficient to take into account, in the FDSC data, a $\kappa(T)$ contribution approximated to a first order polynomial in temperature T, as reported in eq.15. The result for the $100K/s$ case is shown in fig.9, together with a comparison with the data coming from literature [20, 21].

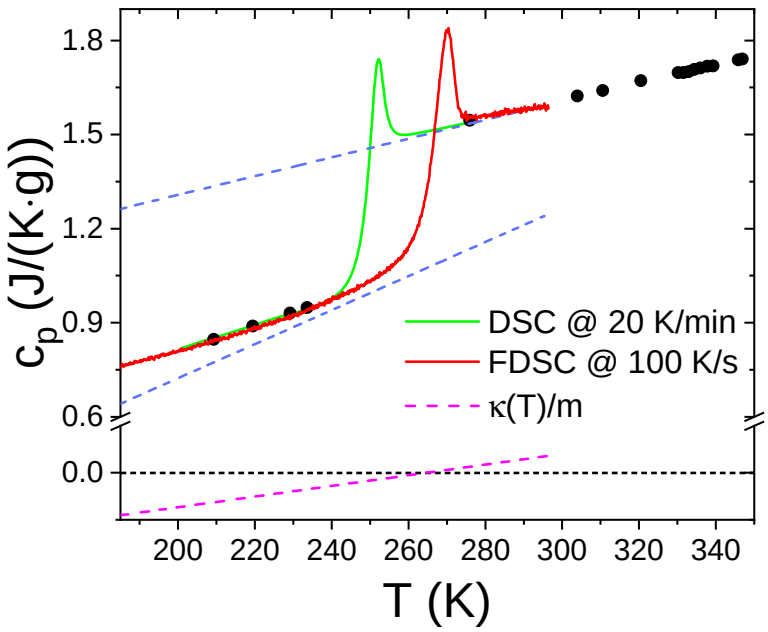

Figure 9: Comparison between our DSC and FDSC specific heat data (green and red lines, respectively) with the ones in literature. Black dots are digitized from [21]; dashed blue lines are from [20]. Note that, for the FDSC scan, the data shown correspond to $c_{p,FDSC} = (C_{FDSC} - \kappa(T))/m$. The dashed magenta line, corresponding to $\kappa(T)/m$, has been estimated according to eq.15.

Note that, in order to obtain $c_{p,FDSC}$ from C_{FDSC}, we have applied eq.15 in the liquid and glassy regions so determining simultaneously the best m, κ_0 and κ_1 parameters in order to minimize the chi-squared in eq.15. We first have obtained m, κ_0 and κ_1 by applying eq.15 only to the FDSC 100 K/s data. The same parameters, used for correcting the thermograms of the other scanning rates, give the results shown in fig.10.

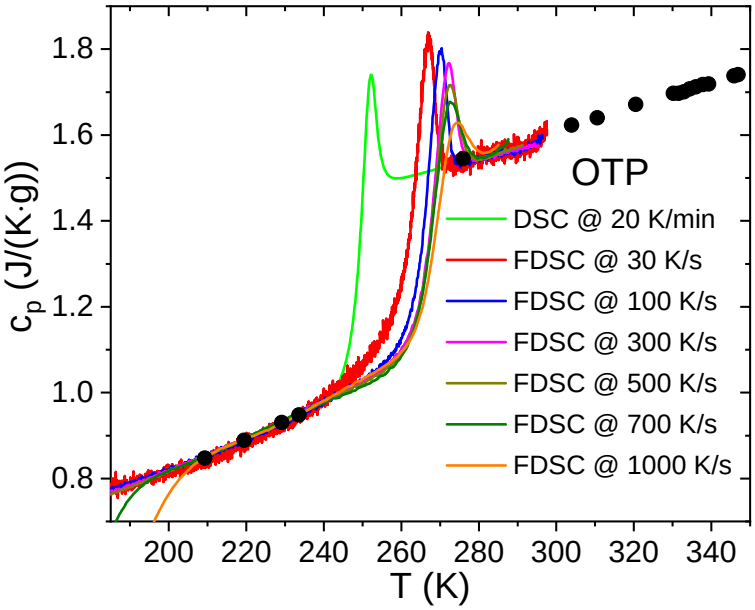

Figure 10: Global plot with the specific heat of the FDSC and DSC measurements of OTP. Black dots have been digitized from [21].

The fitting parameters are: $m = (617 \pm 3)\ ng$, $\kappa_0 = (-289 \pm 4)\ nJ/K$, $\kappa_1 = (0.993 \pm 0.027)\ nJ/K^2$. No constraints have been applied to the fit. It is worth noticing that the m parameter in eq.15 is in good agreement with the value estimated by means of the standard method [1], which is equal to $m \simeq (590 \pm 70)\ ng$ (see fig. $S3$ and Tab. $S2$ of the Supplementary Materials). We want to stress that the very good superposition/alignment of the data, both in the glassy and liquid regions, is obtained with the same $\kappa(T)$ term linear in T for all the scanning rates, through the two regions: this means that the state of the sample (glassy or liquid), at the first order, does not influence the losses. To clarify this point, we recall the expression hypothesized for the losses due to the sample, $HF_{loss}(T, q)$, where we have taken into account a dependence on the scanning rate of the losses, modeled as $HF_0(T, |q|) + \kappa(T)q$. The first term represents the symmetrical component of the heat flow losses, typically used in literature, whereas the second term, proportional to q with its sign, is the one that accounts for the q sign-dependence of the heat flow losses. As regards $\kappa(T)$, we have used a first order approximation in T that has revealed to be sufficient to align simultaneously the FDSC data to the DSC data in the whole temperature interval of the FDSC thermogram, i.e. both in the liquid and glassy regions. A problem still open for FDSC is about the consequences of mechanical stresses between the sample and the membrane (see Sec.1.2.6.3 of [1]). Fortunately, in our experiments we have not revealed any contributions attributable to mechanical stresses.

3.3 Application to low T_g glass-formers

With the same purpose of Sec.3.2, we studied glycerol, a polyol. The peculiarity of this glass-forming material is that it has a low T_g, i.e. $T_g = 190\ K$ at 20 K/min [22].
The lowest accessible temperature for our FDSC is 173 K and it is not possible to measure a well extended glassy line, differently from what happens with OTP. In this particular situation, the E-FDM method is particularly suited because it does not need a glassy line. Thus, symmetrical cooling and heating measurements between 10 and 1000 K/s have been performed and they have been analyzed following the prescriptions given in Secs. 2.2 and 2.3.
After thermal lag and symmetry line correction and fitting the parameters of eq.15, according to the procedure described in the previous section, the FDSC heating thermograms were in good agreement with the DSC specific heat, as it is possible to notice in fig.11.

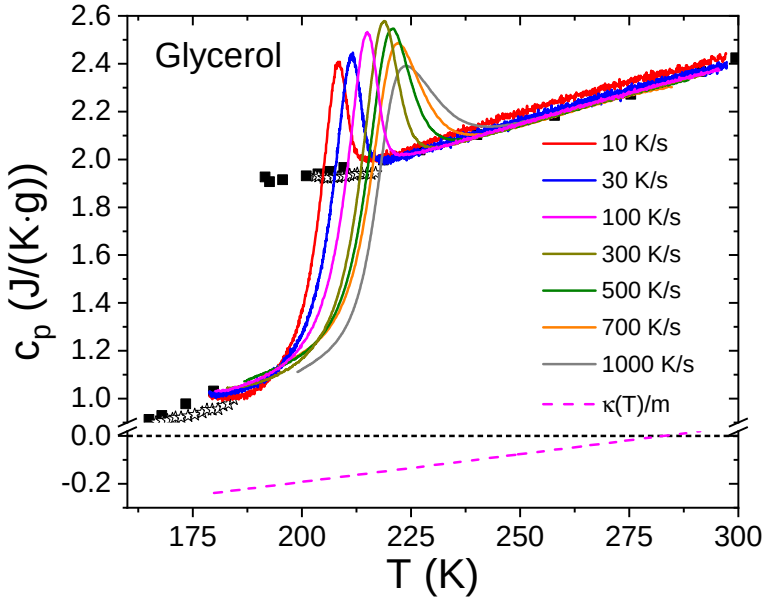

Figure 11: Global plot with the FDSC and DSC specific heats of glycerol. DSC data come from [22] (open stars) and [23] (black squares) The dashed magenta line, corresponding to $\kappa(T)/m$, has been estimated according to eq.15.

The fitting parameters are: $m = (971 \pm 8)\ ng$, $\kappa_0 = (-636 \pm 7)\ nJ/K$, $\kappa_1 = (2.25 \pm 0.04)\ nJ/K^2$. It is worth noticing that in this experimental case, the glassy region collected by FDSC is very narrow and in order to apply eq.15 for fitting the three parameters, we have chosen the measured value at the lowest temperature not affected by transient of the starting of the heating ramp as glassy state value to perform the fit. In practice, this point, combined to the extrapolation of the liquid regime, is sufficient to determine m, κ_0 and κ_1.

Lastly, we present the results obtained on a polymeric system. Even though the study of polymeric materials with FDSC is well established and there are several experiments in literature [1, 8], including how to estimate the thermal lag and heat flow losses with conventional methods, which include the use of standard reference materials, we decided to study a polymer to check for the applicability of this method to this class of organic glass-formers. In the specific case of poly(propylene glycol), with average molecular mass of 4000 Da, (PPG4000), the above-mentioned methods cannot be applied because the sample has a low T_g and a low molecular weight, which puts the specimen very far from the entanglement rubbery plateau, thus the sample is liquid at room temperature and it is impossible to deposit a standard reference material on its top.

The scan rates used are between 100 K/s and 700 K/s and a DSC measurement have been performed at 10 K/min. The FDSC thermograms were subjected to the same correction procedure as exposed in Secs. 2.2 and 2.3, i.e. E-FDM and sample heat flow losses. In the same manner as for OTP, it is possible to recover the agreement between the FDSC and DSC data, by applying thermal lag, symmetry line correction and the correction procedure according to eq.15, as shown in fig.12.

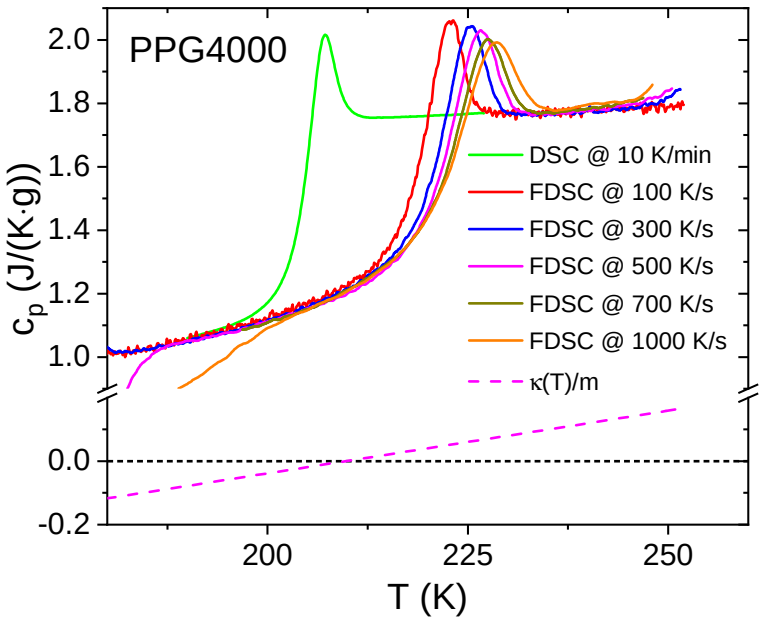

Figure 12: Global plot with the FDSC and DSC specific heats of PPG4000. The dashed magenta line, corresponding to $\kappa(T)/m$, has been estimated according to eq.15.

The fitting parameters are: $m = (314 \pm 3)\ ng$, $\kappa_0 = (-263 \pm 5)\ nJ/K$, $\kappa_1 = (1.24 \pm 0.04)\ nJ/K^2$.

4 Occurence of static and dynamic thermal gradients: beyond correction methods

The presence of static and/or dynamic thermal gradients inside the sample can give rise to distorsions of the measured signal, which are known as *smearing effects* [2]. Here we explore the static smearing effects on the measured heat flow by varying the sensor support temperature (T_{ss}). It is important to notice that this study does not bring to a correction method but to a model-independent procedure to verify the presence of static thermal gradients across the sample and how they affect the thermogram shape.
In literature there are some examples reporting the effect of dynamical thermal gradients [14] and sample mass [24] but there are no studies about the effects of the temperature of the socalled sensor support temperature T_{ss}, which is the temperature of the reference cold finger: the value of T_{ss}, referring to the calorimeter setup, represents also the minimum temperature available for the measurement, and, in our setup, it can be varied between 173 and 313 K. The behavior of the c_p-overshoot peaks at high scanning

rate (above 500 K/s) in figs.10, 11, 12 is compatible with the effect of the dynamical thermal gradient, which increases by increasing the scanning rate: at scanning rates larger than 500 K/s, it results in a broadening and lowering of the overshoot c_p-peak observed on heating, whereas at lower scanning rates, the width and height of the c_p-overshoot peaks are similar, as predicted by TNM simulations of symmetrical heating and cooling scans on fig.1.
To investigate the presence of static thermal gradients on the sample for experiments where the temperature of interest is far from the value of the T_{ss}, we decided to explore different values of T_{ss}, which is the temperature that we control in order to fix the lowest accessible temperature of the measurement. In general, a low T_{ss} is chosen in order to have the widest temperature range for the measurement. This temperature is maintained constant for long time intervals (hours), and it could give rise to static thermal gradients inside the sample.
For this test, we have used, as a probe, the shape of the glass transition peak **measured on heating after cooling at the same scanning rate** for different T_{ss}. Thus, we have carried out symmetrical cooling and heating scans between 298 and 233 K on OTP, varying the sensor support temperature between 173 and 233 K. Before loading the sample on the chip, we have performed its thermocouple calibration at $T_{ss} = 173\ K$. Then we loaded the sample, and made the measurement at that T_{ss}. For the other T_{ss} explored with the same sample and ramp, it was not possible to perform a thermocouples calibration because the sample was already on the chip. As a scanning rate value, we have chosen 100 K/s, which is a factor 5 lower than the scanning rate at which begins to appear a non negligible smearing effects due to dynamic thermal gradients. In fig.13 we show the results on the measured raw heat flow.

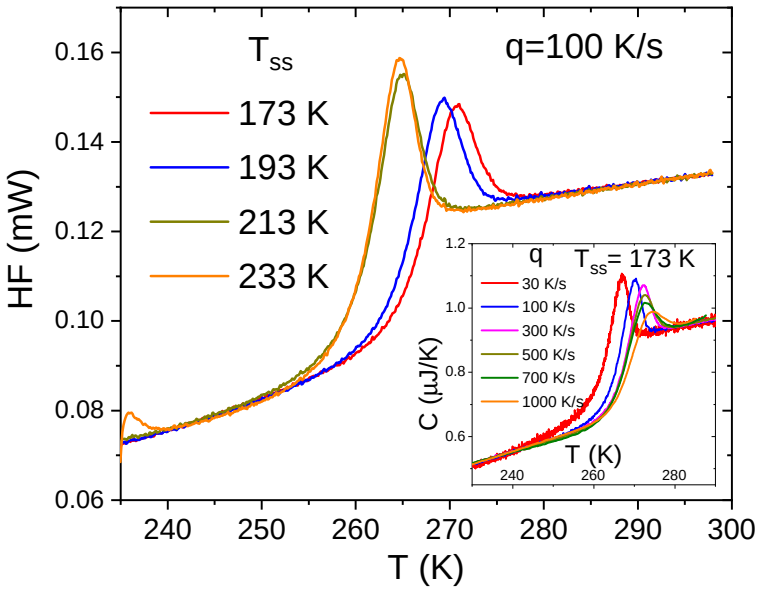

Figure 13: Raw heating scans at 100 K/s at several sensor support temperature T_{ss}, as reported in the plot, showing the presence of a static gradient which shift and broadens the glass transition to higher temperatures when T_{ss} is lowered. Inset: detail from fig.7, which emphasizes the dynamic broadening effect due to the scanning rate, which appears for high values of the scanning rate (> 500 K/s). Note that these measurements have been done with the same T_{ss} and we have varied only the value of the scanning rate.

In fig.13 (main panel), it is possible to notice two main effects: 1) a broadening of the overshoot peaks in correspondence of the lower T_{ss} values; 2) a shift of the glass transition signal to higher temperature in correspondence of the lower T_{ss} values. The two effects, as already suggested in [1], can be explained with the presence of a static thermal gradient across the sample generated by the large distance between the T_{ss} and the measured temperature. We suggest that the broadening effects on the peaks cannot be compensated by any correction procedure, whereas, the temperature shift can be compensated by temperature calibration procedure done for a fixed T_{ss} with reference standard materials. These smearing effects become more evident on increasing the distance between T_{ss} and T_g (or more generally, the temperature of interest), as appears in fig.13. The inset in fig.13 is given for a direct comparison between static and dynamic thermal gradient: the latter become evident at the scanning rates larger than 500 K/s.
To test the mass effect on the thermograms, we have done measurements on a sample with a mass of 82 ng maintaining the $T_{ss} = 173$ K and symmetrical heating and cooling scan between 100 and 1000 K/s. In this case (see fig.$S4$ Supplementary Materials for the thermograms) we obtained that the over-

shoot peak starts broadening and decreasing in amplitude at scanning rates higher than 700 K/s, despite of a reduction in mass of a factor 7 and a τ_{lag} decreasing from 3.3 to 2.3 ms. Even though the mass reduction reduces the thermal lag and the smearing effects, it is evident that we still need to take into account the effects linked to heat propagation and to the static thermal gradients. **Fortunately, these effects do not influence the estimation of the fictive temperature, or its use to determine the thermal lag, because the estimation procedure makes use of well-established glassy and liquid extrapolations and the integration of the thermogram over an extended range to calculate the area between the thermogram and the extrapolated glassy and liquid curves. So, the T_f calculation, based on the energy conservation principle, is not affected by the local shape of the curve.**

Fig.14 shows that, by applying the correction factors obtained from the temperature calibration (see Sec. 2.1 for the standard reference materials used) the peaks superpose, whereas the broadening effect cannot be removed.

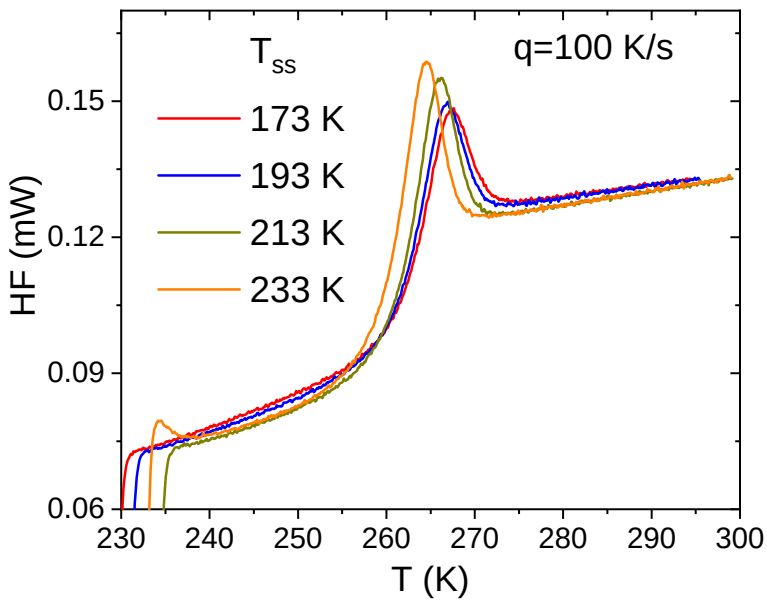

Figure 14: Temperature corrected heating scans at 100 K/s at several sensor support temperatures T_{ss}.

We have performed the same investigation with other two scanning rates, i.e. 300 and 1000 K/s. We have obtained results similar to the 100 K/s case, as it is possible to see in Supplementary Materials from fig.$S7$ to $S10$.
For these three scanning rates, we have inspected the actual scan rate during cooling as a function of the sample temperature. From this inspection, we have made sure to consider only the heeating scans for those samples that, during the cooling, reached the glassy state before the calorimeter lost the control of the cooling scanning rate, i.e. mantaining the cooling rate constant, as it is possible to see in Supplementary Materials from fig.$S5$ to $S6$.
As a final remark, it is worth mentioning that the whole process took at least 2 hours, thus the ageing of the heater should be considered negligible. Moreover, to further test this possibility, we have repeated on the same sample a final measurement at $T_{ss} = 173\ K$ and compared to the one done at the beginning and they resulted the same: so no appreciable ageing of the heaters occurred. The idea behind this set of measurements was to highlight the influence of the T_{ss} on the measure: the temperature shift can be corrected by performing a thermocouple calibration at the desired T_{ss} value, but the smearing effects are not an artifact, they reflect a real static thermal gradient across the sample.

5 Conclusions

In this work we propose an alternative method to correct FDSC thermograms, taking into account the main issues affecting the measurement, i.e. dynamical thermal gradients, heat flow losses due to the sample and static thermal gradients.
The correction of dynamical thermal lag via the first derivative method (FDM) or the extended one (E-FDM) is needed for a specific class of organic molecular compounds. Indeed, as noted also by Monnier et al. [8] with a polymeric material, a dynamical thermal gradient is present in each measurement, even at low scanning rates. In the case of organic molecular glass-formers, the standard procedures, based on the estimation of the fictive temperature or the use of a piece of indium placed on top of the sample, cannot be applied because: i) the system has a low T_g, and thus no clear glassy line is measured, and the T_f cannot be calculated; ii) the sample is liquid at room temperature and it is impossible to deposit a piece of indium on its top; iii) the sample degrades/evaporates before reaching the melting temperature of indium, used to estimate the dynamical thermal gradient. The advantage of FDM and E-FDM is that it is possible to obtain the temperature lag correction by directly using the temperature of the maximum slope points of the glass transition heat flow curves on heating and cooling

and the temperature of the overshoot peak on heating. It is worth mentioning that FDM can be used after verifying that no significative broadening exists, i.e. the temperature difference ($\Delta T_{2,exp}$) between the point of maximum slope on heating and the point of maximum of the overshoot peak is nearly constant with the scan rate. When there is a non-negligible variation of $\Delta T_{2,exp}$ with the scan rate, it is sufficient to use the E-FDM to take into account the broadening affecting $\Delta T_{1,exp}$, so correctly determining τ_{lag}. FDM and E-FDM have also the advantage that do not require the use of a reference material and do not need a well-extended glassy line, necessary for the application of the T_f method, like we observed for glycerol in Sec.3.3.

Applying the symmetry line correction, as usually done in literature, we have found that the FDSC curves superpose in the liquid and glassy regimes but a scaling of the heat flow with the estimated mass value is not sufficient to align the FDSC data with the DSC data in the glassy and liquid regions. It is worth mentioning that, recently, some empiric data treatments for thermogram alignment have been published [25, 26]. These works propose a simple and effective procedure to correct the curves after symmetry line subtraction: the correction is practically achieved by means of a combination of translation and rotation of a selected thermogram with respect to a reference one. Even though they make possible to superpose the FDSC thermograms at several scanning rates, a motivation of the rescaling to the value of the specific heat obtained from the DSC is still lacking. Here we have proposed a new approach based on a novel interpretation of the heat flow losses due to the sample which takes into account the sign of the scanning rate. In this new interpretation of the heat flow losses, the contribution of the heat flow losses linear in temperature and proportional to the scanning rate allows to obtain a good agreement between the FDSC and DSC specific heat data.

Finally, the presence of static gradients, coming from the distance between the T_{ss} and the temperature of interest, has been investigated by means of the use of the observed glass transition peak shape, using a fixed scan rate value but different T_{ss} values. This method has allowed to detect the presence and the entity of the static thermal gradients on the measured heat flow.

In conclusion, we propose new solutions for FDSC thermogram correction which account for dynamical thermal lag, heat flow losses due to the sample and static thermal gradients due to T_{ss}. These solutions can be applied to every glass-forming system that has the glass transition in the temperature interval of the measurement, and are able to recover the agreement between the FDSC and DSC specific heat data.

6 Acknowledgments

We acknowledge CISUP for the access to Mettler Toledo Flash DSC 2^+.

References

[1] C. Schick, V. Mathot, *Fast scanning calorimetry*, Springer Nature 2016. doi: $https://doi.org/10.1007/978-3-319-31329-0$.

[2] G. W. H. Höhne, W. F. Hemminger, H.-J. Flammersheim, *Differential scanning calorimetry*, Springer Berlin 1996. doi: $https://doi.org/10.1007/978-3-662-06710-9$.

[3] A. Toda, *Heating rate dependence of melting peak temperature examined by DSC of heat flux type*, J. Therm. Anal. Calorim. (2016), 123, 1795-1808. doi: $https://doi.org/10.1007/s10973-015-4603-3$.

[4] A. A. Minakov, *Temperature gradients in ultrafast thin-film nanocalorimetry*, Thermochim. Acta (2019), 677, 32-41. doi: $https://doi.org/10.1016/j.tca.2019.02.014$.

[5] S. Van Herwaarden, E. Iervolino, F. Van Herwaarden, T. Wijffels, A. Leenaers, V. Mathot, *Design, performance and analysis of thermal lag of the UFS1 twin-calorimeter chip for fast scanning calorimetru using the Mettler-Toledo Flash DSC* 1, Thermochim. Acta 522 (2011) 46-52. doi: $10.1016/j.tca.2011.05.025$.

[6] J. E. K. Schawe, *Temperature correction at high heating rates for conventional and fast differential scanning calorimetry*, Thermochim. Acta 698 (2021) 178879. doi: $https://doi.org/10.1016/j.tca.2021.178879$.

[7] A. A. Minakov, C. Schick, *Integro-Differential Equation for the Non-Equilibrium Thermal Response of Glass-Forming Materials: Analytical Solutions*, Symmetry 13(2) (2021) 256. doi: $https://doi.org/10.3390/sym13020256$.

[8] X. Monnier, A. Saiter, E. Dargent, *Physical aging in PLA through standard DSC and fast scanning calorimetry investigations*, Thermochim. Acta 648 (2017) 13-22. doi: $https://doi.org/10.1016/j.tca.2016.12.006$.

[9] J. E. K. Schawe, *Measurement of the thermal glass transition of polystyrene in a cooling rate range of more than six decades*, Thermochim. Acta 603 (2015) 128-134. doi: $http://dx.doi.org/10.1016/j.tca.2014.05.025$.

[10] I. M. Hodge, A. R. Berens, *Effects of Annealing and Prior History on Enthalpy Relaxation in Glassy Polymers. 2. Mathematical Modeling*, Macromol. 15 (1982) 762-770. doi: $https://doi.org/10.1021/ma00231a016$.

[11] S. Weyer, M. Merzlyakov, C. Schick *Application of an extended Tool-Narayanaswamy-Moynihan model. Part 1. Description of vitrification and complex heat capacity measured by temperature-modulated DSC*, Thermochim. Acta 377 (2001) 85-96. doi: $https://doi.org/10.1016/S0040-6031(01)00543-3$.

[12] Y. Z. Chua, G. Schulz, E. Shoifet, H. Huth, R. Zorn, J. W. P. Scmelzer, C. Schick, *Glass transition cooperativity from broad band heat capacity spectroscopy*, Colloid. Polym. Sci. 292 (2014) 1893-1904. doi: $https://doi.org/10.1007/s00396-014-3280-2$.

[13] J. W. P. Schmelzer, T. V. Tropin, V. M. Fokin, R. Zhang, A. Abdelaziz, Y. Z. Chua, V. Madhavi, T. D. Shaffer, C. Schick, *Correlation between glass transition temperature and the width of the glass transition interval*, Int. J. Appl. Glass Sci. 10 (2019) 502-513. doi: $http://dx.doi.org/10.1016/j.tca.2015.07.009$.

[14] R. Svoboda, *Glass transition kinetics measured by fast scanning calorimetry - Effect of thermal gradients*, J. Therm. Anal. Calorim. 122 (2015) 985-995. doi: $10.1007/s10973-015-4803-x$.

[15] E. Zhuravlev, C. Schick, *Fast scanning power compensated differential scanning nano-calorimeter: 2. Heat capacity analysis*, Thermochim. Acta 505 (2010) 14-21. doi: $10.1016/j.tca.2010.03.020$.

[16] D. N. Bolmatenkov, M. I. Yagofarov, T. A. Mukhametzyanov, M. A. Ziganshin, C. Schick e B. N. Solomonov, *A new method for heat capacity determination in supercooled liquid state using fast scanning calorimetry: Thermochemical study of* $9,9'$*-bifluorenyl*, Thermochim. Acta 694 (2020) 178805. doi: $https://doi.org/10.1016/j.tca.2020.178805$.

[17] C. R. Quick, J. E. K. Schawe, P. J. Uggowitzer, S. Pogatscher, *Measurement of specific heat capacity via fast scanning calorimetry — Accuracy and loss corrections*, Thermochim. Acta 677 (2019) 12-20. doi: $https://doi.org/10.1016/j.tca.2019.03.021$.

[18] C. T. Moynihan, A. J. Easteal, M. A. DeBolt, *Dependence of the Fictive Temperature of Glass on Cooling Rate*, J. Am. Ceram. Soc. 59(1-2) (1976) 12-16. doi: $https://doi.org/10.1111/j.1151-2916.1976.tb09376.x$.

[19] S. Gao, S. L. Simon, *Measurement of the limiting fictive temperature over five decades of cooling and heating rates*, Thermochim. Acta 603 (2015) 123-127. doi: $http://dx.doi.org/10.1016/j.tca.2014.08.019$.

[20] M. I. Yagofarov, S. E. Lapuck, T. A. Mukhametzyanov, M. A. Ziganshin, C. Schick e B. N. Solomonov, *Application of fast scanning*

calorimetry to the fusion thermochemistry of low-molecular-weight organic compounds: Fast-crystallizing m-terphenyl heat capacities in a deeply supercooled liquid state, Thermochim. Acta 668 (2018) 96-102. doi: $https://doi.org/10.1016/j.tca.2018.08.015$.

[21] S. S. Chang, A. B. Bestul, *Heat Capacity and Thermodynamic Properties of o-Terphenyl Crystal, Glass, and Liquid*, J. Chem. Phys. 56(1) (1972) 503-516. doi: $https://doi.org/10.1063/1.1676895$.

[22] L.-M. Wang, V. Velikov, C. A. Angell, *Direct determination of kinetic fragility indices of glassforming liquids by differential scanning calorimetry: Kinetic versus thermodynamic fragilities*, J. Che. Phys. 117 (2002) 10184. doi: $https://doi.org/10.1063/1.1517607$.

[23] G. E. Gibson, W. F. Giauque, *The third law of thermodynamics. Evidence from the specific heats of glycerol that the entropy of a glass exceeds that of a crystal at the absolute zero*, J. Am. Chem. Soc. 45(1) (1923) 93-104. doi: $https://doi.org/10.1021/ja01654a014$.

[24] G. V. Poel, D. Istrate, A. Magon, V. Mathot, *Performance and calibration of the Flash DSC 1, a new, MEMS-based fast scanning calorimeter* J. Therm. Anal. Calorim. 110 (2012), 1533-1546. doi: $10.1007/s10973-012-2722-7$

[25] A. A. Abate, D. Cangialosi, S. Napolitano, *High throughput optimization procedure to characterize vitrification kinetics*, Thermochim. Acta 707 (2022) 179084. doi: $https://doi.org/10.1016/j.tca.2021.179084$.

[26] P. Cebe, B. P. Partlow, D. L. Kaplan, A. Wurm, E. Zhuravlev, C. Schick, *Using flash DSC for determining the liquid state heat capacity of silk fibroin*, Thermochim. Acta 615 (2015) 8-14. doi: $http://dx.doi.org/10.1016/j.tca.2015.07.009$.